Chemical capacitance of nanoporous-nanocrystalline TiO_2 in a room temperature ionic liquid

Francisco Fabregat-Santiago,*[a] Hyacinthe Randriamahazaka,*[b] Arie Zaban,[c] Jorge Garcia-Cañadas,[a] G. Garcia-Belmonte[a] and Juan Bisquert[a]

Received 12th January 2006, Accepted 17th February 2006
First published as an Advance Article on the web 28th March 2006
DOI: 10.1039/b600452k

The electrochemical behaviour of nanoporous TiO_2 in a room temperature ionic liquid (RTIL), 1-ethyl-3-methylimidazolium bis((trifluoromethyl)sulfonyl)amide (EMITFSI), was investigated by cyclic voltammetry (CV) and impedance spectroscopy. Exponentially rising currents in voltammetry were attributed to the charging/discharging of electrons in the TiO_2 film and a charge transfer mechanism. The main features of the voltammetry and impedance followed the same trends in the ionic liquid as in other organic solvents and also in aqueous electrolytes. In the presence of lithium ions, the onset potential of the charge accumulation increased due to the change of the initial position of the TiO_2 conduction band. The results show that substitution of organic solvents contained in solar cells, supercapacitors or other electrochemical devices is in general feasible, though requires some adjustment in the electrolyte composition for optimal performance.

1. Introduction

Nanoporous metal oxide electrodes have been utilized in many applications such as photovoltaics, photocatalysis and energy storage (batteries and supercapacitors). An important material in this respect is titanium dioxide, whose combination of semiconducting properties and chemical stability makes it a candidate for use in, for example, rechargeable batteries [1–3] and solar cells.[4–6] In the field of photovoltaics, dye-sensitized solar cells (DSCs) are attractive due to their high-energy conversion efficiency and low production cost.

Room temperature ionic liquids (RTILs) have been the focus of many recent scientific investigations because of their physical and chemical properties.[7–15] They are promising for many applications in electrochemical systems such as actuators, batteries, supercapacitors, electrochromic windows and displays, photovoltaic cells and light-emitting electrochemical cells. From an electrochemical aspect, ionic liquids have excellent properties, in particular high-ionic conductivity and wide potential windows. They are also non-volatile and non-flammable and have high thermal stability. Some ionic liquids have the advantage that they can be obtained in a very dry state, which is especially suitable for electrochemical applications from which moisture must be excluded over long periods of operation. The utility of RTILs for DSCs has been reported recently,[16–18] avoiding such problems as leakage and evaporation of the organic solvent and high-temperature instability.

Electrochemical cyclic voltammetry (CV) and impedance spectroscopy (IS) are useful tools for investigating the effects of electrolyte composition on the extent and nature of electron accumulation and the charge compensation in nanostructured metal oxide electrodes. Understanding these processes is essential for performance optimization of electrochemical and photoelectrochemical nanostructured devices. In this work, we utilize these two techniques to examine the charging/discharging processes within nanoporous-nanocrystalline TiO_2 and the effect of a current loss due to an irreversible charge transfer. The results will be interpreted using methods previously developed for liquid electrolyte based nanoporous electrodes.[19] First, we shall compare the electrochemical behaviours of nanoporous TiO_2 in a RTIL and in a standard liquid electrolyte, propylene carbonate (PC). Then, we analyse the effect of adding lithium salt, $Li(CF_3SO_2)_2N$, on the CV response. Finally, we will make a deeper analysis of the electrochemical response of the TiO_2 film in RTILs and Li^+ salt by means of IS.

2. Experimental

The RTIL used in this work was 1-ethyl-3-methylimidazolium bis((trifluoromethyl)sulfonyl)amide (EMITFSI), which exhibits a high ionic conductivity. In measurements with lithium the salt lithium bis((trifluoromethyl)sulfonyl)amide ($Li(CF_3SO_2)_2N$ or LiTFSI) was used.

The synthesis of EMITFSI, (Fig. 1), was achieved using a previously published procedure.[7] The 3,4-ethylenedioxythiophene (EDOT) monomer was provided by Bayer AG and distilled prior to use. $LiClO_4$ was supplied by Fluka. LiTFSI, Acetonitrile (ACN) and propylene carbonate (HPLC grade)

[a] *Departament de Ciències Experimentals, Universitat Jaume I, 12071 Castelló, Spain. E-mail: fabresan@exp.uji.es; Fax: +34 964 728066; Tel: +34 964 728024*
[b] *Interfaces, Traitements, Organisation et Dynamique des Systèmes (ITODYS), CNRS-UMR 7086, Université Paris 7 - Denis Diderot, 1 rue Guy de la Brosse, 75005 Paris, France. E-mail: randria@itodys.jussieu.fr; Fax: +33 144 276814; Tel: +33 144 276107*
[c] *Department of Chemistry, Bar-Ilan University, Ramat-Gan 52900, Israel*

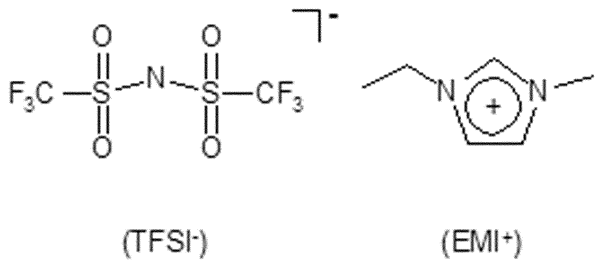

Fig. 1 Structures of bis((trifluoromethyl)sulfonyl)amide, $TFSI^-$, (a) and 1-ethyl-3-methylimidazolium, EMI^+, (b).

were obtained from Aldrich. The synthesis and characterization of the TiO_2 is reported elsewhere.[20]

The electrochemical experiments with the RTIL were performed in a sandwich configuration as described in Fig. 2. This cell configuration was used in order to minimize the quantity of RTIL used during each experiment. In all the cases, the geometric area of the nanostructured electrode was 1 cm^2. The working electrode was a nanostructured TiO_2 deposited on an optically transparent electrode (F-doped SnO_2), TCO. The same TCO, electrically separated from the area in which the film is deposited, was used as pseudo-reference. The counter-electrode consisted of electrochemically deposited poly(3,4-ethylenedioxythiophene), PEDOT, on TCO. The electrodeposition was performed in a 0.1 M $LiClO_4$ in acetonitrile solution containing the monomer as described in a previous study.[21] After its preparation, the PEDOT electrode was washed with acetonitrile and cycled in a monomer free solution with 0.1 M $LiClO_4$. When a stable CV was obtained, the PEDOT electrode was oxidized electrochemically.

The measurements of the samples containing liquid based electrolyte, PC, were carried out in a three electrode configuration, with the TiO_2 working electrode, a platinum electrode as a counter-electrode and Ag/AgCl reference electrode. The supporting salt was 0.1 M KPF_6 (Aldrich). The cyclic voltammetry experiments were performed on an EG&G Princeton Applied Research model 273A Potentiostat/Galvanostat or on an Autolab General Purpose Electrochemical (AUT30.FRA2-AUTOLAB, Eco Chemie, B.V., The Netherlands), with which we also carried out the impedance measurements.

In this work, with the aim of a better comparison between the two electrolytes, all the potentials are referenced to Ag/AgCl. Thus, to reference the potentials measured for ionic liquid samples, the potentials of TCO in pure RTIL and RTIL with Li^+ were measured in open circuit conditions *vs.* Ag/AgCl and the obtained values used to correct the data to the same reference. No potential drift was observed over the 1 h measurements.

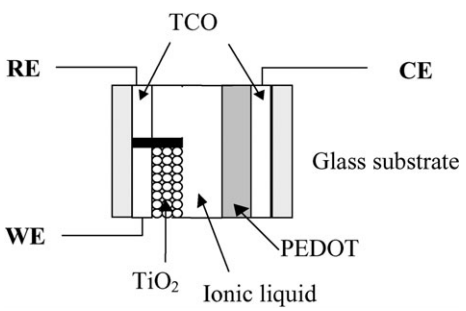

Fig. 2 Schematic representation of the electrochemical cell. RE is the reference electrode, WE is the working electrode and CE is the counter-electrode.

3. Results and discussion

CVs of nanoporous TiO_2 films immersed in RTIL and in the liquid electrolyte are shown in Fig. 3. We report the following observations.

The current shows a plateau at the potentials where the TiO_2 is an insulator (around 0 V). Here, the electrical response is dominated by the Helmholtz capacity of the uncovered TCO/solution interface at the bottom of the TiO_2 film.[22] This capacity has a constant value of 4 μF cm^{-2} in the case of the molten salt and 11 μF cm^{-2} for the liquid electrolyte. The difference may be explained by the different dielectric constants of the two media and the size of the positive ions, K^+ and EMI^+. When the voltammetry is confined to this region and swept at different rates a linear relationship is observed between the measured current and the sweep rate (Fig. 4). At

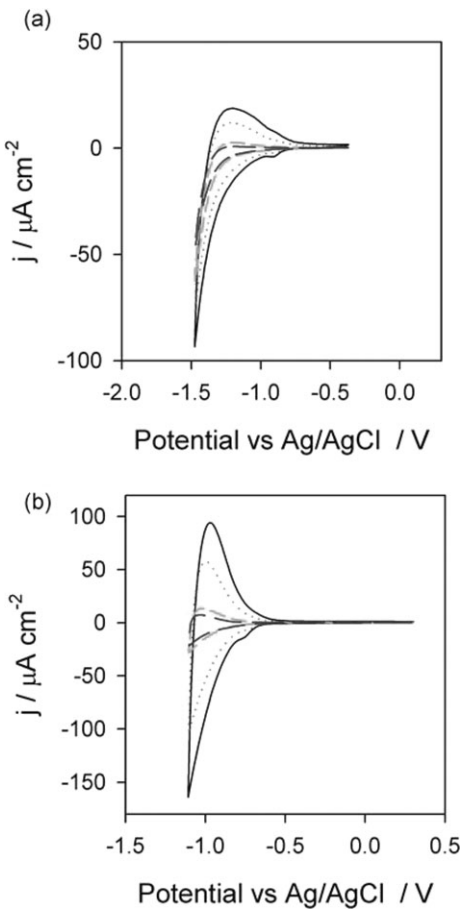

Fig. 3 Cyclic voltammetry of nanoporous titanium dioxide films in 0.1 M LiTFSI in RTIL (a) and 0.1 M KPF_6 in PC (b). Both present the same shape, the only difference being a shift in the potentials of the CV. The separate lines represent different current sweep rates: 100 mV s^{-1} (—); 50 mV s^{-1} (···); 10 mV s^{-1} (--); 5 mV s^{-1} (– –).

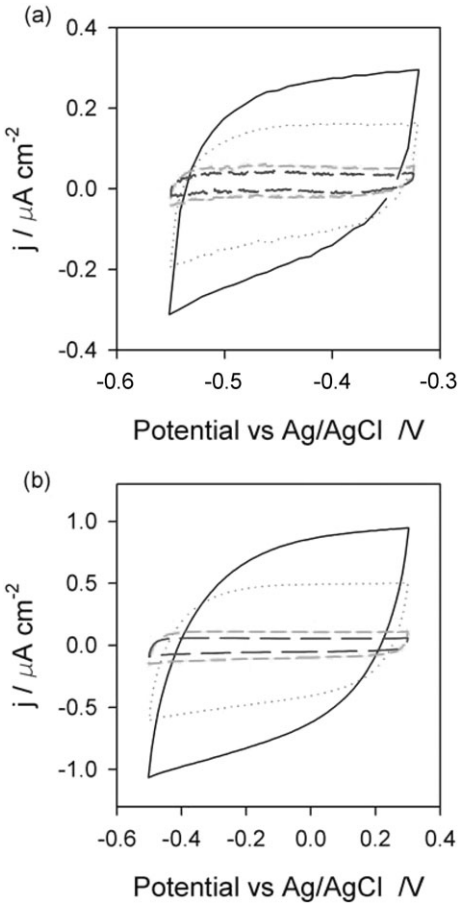

Fig. 4 Cyclic voltammetry of nanoporous titanium dioxide films in 0.1 M LiTFSI in RTIL (a) and 0.1 M KPF_6 in PC (b) confined to the region where the capacity of the TCO/solution dominates. The separate lines represent different current sweep rates: 100 mV s^{-1} (—); 50 mV s^{-1} (···); 10 mV s^{-1} (--); 5 mV s^{-1} (– –).

high speeds the end of the plateau is rounded due to the presence of a resistance (larger in the system with PC than for the one with RTIL) originating from the sum of the TCO and electrolyte resistances, which are connected in series with this nearly constant capacitor.[19,23,24]

At the more negative potentials, the cathodic current displays an exponentially rising behaviour that is transformed into a peak when the direction of the voltammetry is reversed to anodic. As the sweep rates become slower the height of the anodic peak diminishes until, at very low rates, it disappears. As explained below, the origin of this behaviour is the sum of two contributions: the charging/discharging of electrons in the film and a charge transfer mechanism.

It has been shown in several works that charge accumulation in TiO_2 generates an exponentially dependent capacity.[19,25–29] This chemical capacitance[30–32] is proportional to the derivative of the density of electrons in the TiO_2, n, with respect to the Fermi level, E_{F_n}, which depends on the potential as $V = (E_{F_n} - E_{F_0})/e$ (see Fig. 5),

$$C = -\frac{\partial Q}{\partial V} = e^2 \frac{\partial n}{\partial E_F} \qquad (1)$$

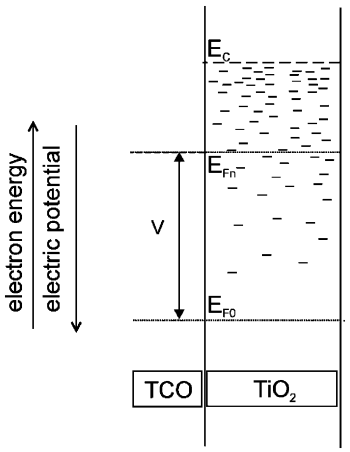

Fig. 5 Scheme of the electron density in TiO_2. As the Fermi level approaches the conduction band due to the applied potential then n, and thus the capacity, increase exponentially.

where e is the charge of an electron. The electron density depends on the Fermi level as

$$n = n_0 \, e^{\alpha(E_{Fn} - E_{F0})/k_B T} \qquad (2)$$

where k_B is the Boltzmann constant and T is the temperature, E_{F_0} the position of the Fermi level in equilibrium and α is a constant accounting for bandgap localized states and can take values ≤ 1. Thus, from eqn (1) and (2), we can write

$$C = C_0 e^{-\alpha e V/k_B T} \qquad (3)$$

where $C_0 = Ae^{-\alpha E_{cb}/k_B T}$ is a constant that depends on the position of the conduction band edge of TiO_2, E_{cb}. The capacitance increases exponentially with negative bias and yields the characteristic voltammetry shown in Fig. 3.

At a certain potential, the chemical capacitance associated with the electron population becomes larger than the Helmholtz capacitance of the substrate/solution interface and dominates the capacitive component of the film. This effect determines the shape of the CV at high enough negative potentials and sweep rates such as those plotted in Fig. 3. The shape of the anodic peak is a function of both the series and the charge transfer resistances previously mentioned.[19] At return potentials below the activation of the charging of the semiconductor and the charge transfer, the Helmholtz capacity dominates (Fig. 4). It is important to remark here that the anodic peak of the CV in Fig. 3 is not related to a single-energy redox process. Indeed, this kind of process relating to the charging of a distribution of states does not yield a cathodic peak at more negative potentials.

The charge transfer process is mainly related with irreversible electron leakage to acceptors such as oxygen in the solution. Charge transfer dominates the CV at low scan rates and at intermediate return potentials (Fig. 6) where the current associated with the TiO_2 capacitance is small. The main difference between the shapes of the voltammetry in Fig. 3a and b is the voltage at which the transition occurs from the Helmholtz-controlled current to the exponentially rising current.

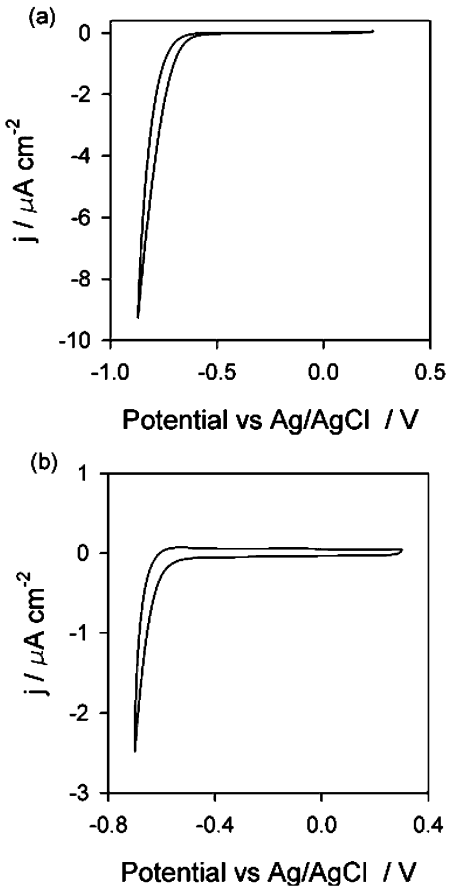

Fig. 6 Slow scan rate cyclic voltammetry of nanoporous titanium dioxide films in 0.1 M LiTFSI in RTIL at 1 mV s^{-1} and (a) 0.1 M KPF_6 in PC at 5 mV s^{-1} and (b) at the most negative potentials of these CV's, leakage currents dominate over capacitive.

This onset potential is controlled by the initial position of the conduction band of the TiO_2 with respect to the equilibrium position at open circuit, E_{F_0}. This position is determined by the film preparation parameters and the electrolyte composition, *i.e.* the type of the solvent and ions used and their concentration.[19,33–35] From this result we can expect that the different environment at the surface of the TiO_2 will necessitate re-optimizing the components added to the solvent when the liquid electrolytes are substituted by a molten salt in a device.

In the following section we discuss the influence of the Li^+ ions on the electrochemical response of TiO_2 in EMITFSI. Li^+ is an ion commonly used in applications such as dye sensitized solar cells to screen the charge in the semiconductor. It is well known that in liquid electrolytes it has other effects such as lowering the conduction band edge position to a greater extent than other, larger cations.[33,35]

Fig. 7 shows the CV patterns of a nanoporous TiO_2 electrode in the presence and absence of Li^+ for small return potentials. As expected, the exponential rising of the current begins at less negative potential when Li^+ ions are present in EMITFSI. In addition, the presence of the Li^+ ions in the EMITFSI results in a change of the Helmholtz capacity of the system. This change is shown by adjusting the sweep rate of

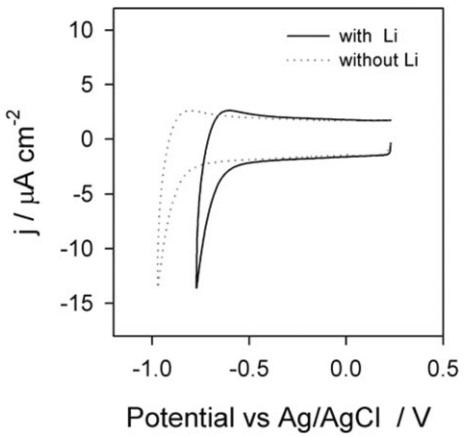

Fig. 7 Shift in the CV of TiO_2 films in RTIL with (—) and without (···) LiTFSI. The voltammetry of the electrolyte with Li^+ was taken at a scan rate of 100 mV s^{-1} while the one without was taken at 400 mV s^{-1}. The differences in the Helmholtz capacitance deducted from this plot may be explained by the different size of the Li^+ and EMI^+ cations.

the two CVs to values that produce similar currents. A scan rate that is 4 times slower when Li^+ is present compared with the Li^+ free RTIL shows that the Helmholtz layer capacitance increases by a factor of 4 upon Li^+ addition. Both effects are related with the different size of the two ions, EMI^+ and Li^+.[33,35] With regard to the onset of the exponential current increase, the smaller the ion size, the bigger is the positive shift of the TiO_2 conduction band edge. Consequently, in the presence of lithium, C_0 of eqn (3) is bigger and the onset of charge accumulation during the cathodic scan occurs at a more positive potential. Thus, the conduction band edge level of TiO_2 is controlled by surface interactions. Regarding the Helmholtz layer capacitance, smaller ions involve a thinner Helmholtz double layer and, therefore, a larger capacitance associated to it.

Another possible effect, though with relatively smaller impact than the size effect over the CV, is the reported specific interaction of imidazolium cation on nanoporous TiO_2 surface.[36] It must be borne in mind that despite the large size of EMI^+ compared with that of Li^+, the concentration of EMI^+ was very high in our experimental conditions. Thus, the surface interaction competition involving Li^+ and EMI^+ on TiO_2 can be affected by the dynamics of the surface rearrangement. In this context, the surface rearrangement processes can be viewed as the change of the surface concentration of cations involved in the specific interactions with the TiO_2 surface. The detailed analysis of this phenomenon is reserved for future work.

The results presented and discussed above may be analysed more deeply by using IS. We have measured the impedance of a TiO_2 cell in RTIL with Li^+ in the same range as the CV measurements. Similar results (but displaced in potential) may be expected for the sample with pure RTIL as its CV has the same shape.

In Fig. 8 we present the values of the charge transfer resistance and capacitance of a TiO_2 film obtained at the potentials where the semiconductor produced a measurable

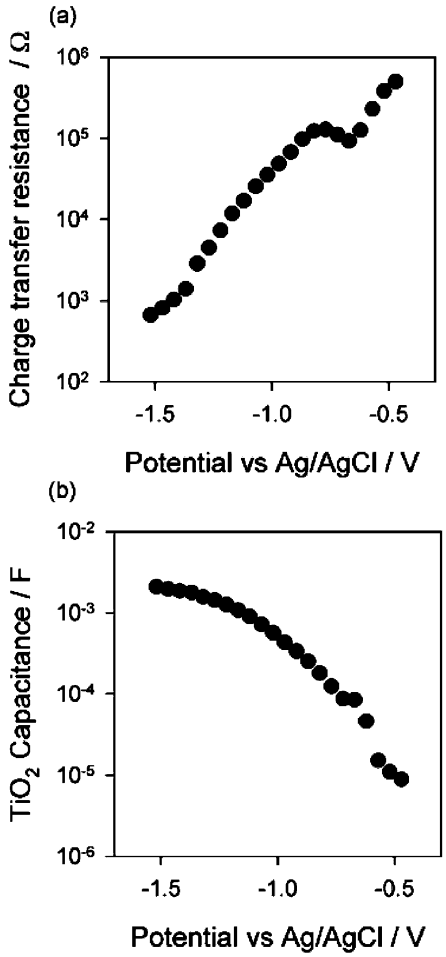

Fig. 8 Charge transfer resistance (a) and TiO_2 capacitance (b) obtained from impedance as a function of the applied potential in a film immersed in RTIL with 0.1 M LiTFSI.

response. At more positive potentials, as described for CV, Helmholtz capacitance dominated the impedance spectra.

In the range of potentials shown in Fig. 8a, the charge transfer resistance varies exponentially from nearly 1 MΩ to less than 1 kΩ with a small valley at 0.7 V. In the same range, the TiO_2 film capacitance has an exponential rise as described previously, with a peak also at 0.7 V. The valley and peak appearing in both graphs corresponds to the presence of a well known Ti^{3+} intraband localized state,[37,38] which is more prominent and easy to observe in CV when, as in our case, the sample is aged (Fig. 9). Note that contrary to many cases in aqueous electrolytes, here the charging and discharging of these states demonstrates significant reversibility. This indicates a low charge transfer from this state to the electrolyte (low losses) and a good enough conductivity of the TiO_2 at these potentials to allow full discharge of the state.

In Fig. 8b the capacitance tends to saturate into a constant value. This value is the Helmholtz capacity of the total surface of the TiO_2 film, which allows an estimate of the total to geometric surface ratio of $\approx 200:1$. If we take the data far from this saturation and perform the calculations in ref. 19, from these capacitance data we can roughly estimate that the

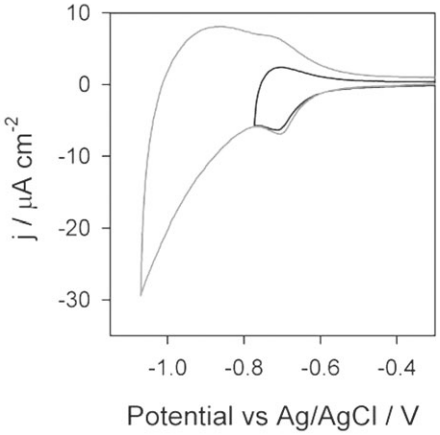

Fig. 9 Cyclic voltammetries at different return potentials of a TiO_2 film in a RTIL with 0.1 M LiTFSI solution. The peak attributed to intraband Ti^{3+} states (arrows) rises with cycling. Note, that in RTIL the peak seems quite reversible.

conduction band edge is located at around −1.35 V *vs.* Ag/AgCl. Note, that when the saturation level is approached most of the overpotential drops in the electrolyte layer but the Fermi level in the semiconductor may hardly approach the conduction band edge.

If we extrapolate the results of Fig. 8 to the CV of the sample in RTIL without Li^+, we find that the combination of the high leakage and saturation of capacity is the reason why the anodic current peak of Fig. 3a is not as large as in the case of liquid electrolyte, Fig. 3b.

A final remark about the models used to fit impedance data should be made here. At the cathodic limit of potential, the impedance can be modelled by a resistance in series with the parallel combination of the charge transfer resistance of electrons from TiO_2 to acceptors in the electrolyte and the capacity of the TiO_2 film. At the anodic limit, the equivalent circuit is the same but now the capacity and the transfer

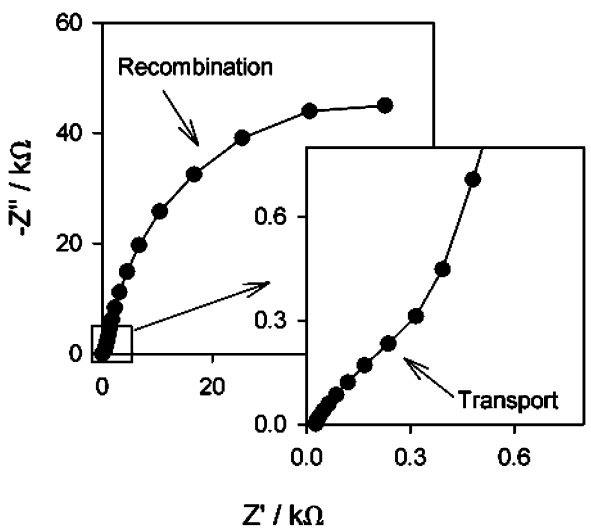

Fig. 10 Typical impedance spectrum of nanoporous TiO_2 at potentials of transition varying from the insulating to conducting state.

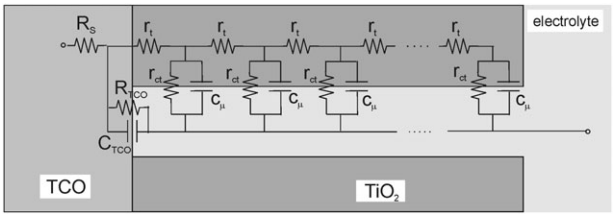

Fig. 11 Complete transmission line model used to fit the data. At very negative potentials $r_t \rightarrow 0$ and the transmission line is reduced to the parallel combination of the chemical capacitance of TiO_2 and the charge transfer from semiconductor to electrolyte, $C_\mu = c_\mu L$, $R_{ct} = r_{ct}/L$. At positive potentials, $r_t \rightarrow \infty$ and the only contributions are those from the TCO/electrolyte interface.

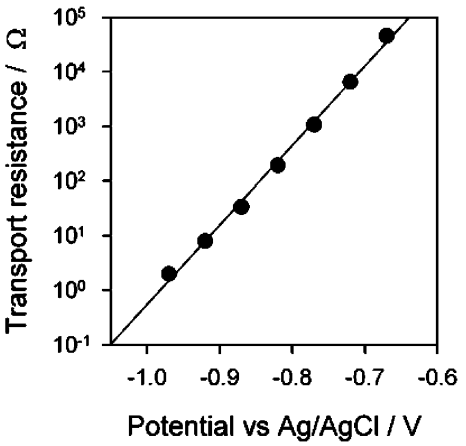

Fig. 12 Transport resistance of TiO_2 film in a RTIL with 0.1 M LiTFSI solution as a function of the applied potential.

resistance have their origin in the Helmholtz layer of the substrate and its charge losses, which are very low and thus, R_{ct} is very high. At intermediate potentials the TiO_2 changes from an insulating to a very conductive media and from a depleted to a charged system. The characteristic impedance spectra during these transitions (Fig. 10) may be fitted by using transmission line based models as described elsewhere[35,39] (Fig. 11). These models allow decoupling transport and recombination resistances and electron accumulation capacitance in this intermediate region, which in our case ranged from −0.7 to −1 V. The evolution of electron transport resistance in TiO_2, $R_t = r_t L$, in this range is shown in Fig. 12. The slope gives the transport resistance as 15.1 V^{-1} (or 66 mV per decade), very near to the theoretical value 17 V^{-1} (or 59 mV per decade) for a pure conduction band or multiple trapping transport mechanisms, and very similar to the values obtained for nanoporous TiO_2 films in acidic aqueous solutions,[39] which also exhibit the same CV patterns.[19]

4. Conclusions

In the complete potential range studied, the behaviour of the nanoporous-nanocrystalline TiO_2 modified electrode follows the same trends in each of the three media employed (RTIL, PC or aqueous). Also, an anodic shift (in potential scale) or a decrease of the energy level (energy scale) of the conduction band of TiO_2 is observed in the presence of Li^+ in EMITFSI. This effect is explained by the competitive surface interactions of the imidazolium cation of RTIL and Li^+ on TiO_2 due to the different ionic size. The ionic size is also responsible for a change in the Helmholtz capacitance at the interface between uncovered substrate and the solution.

These results indicate that RTIL is a suitable medium to substitute any solvent used in TiO_2-based devices, such as solar cells, supercapacitors, *etc*. However, the change of the conduction band due to the differences in surface interactions must be considered and the additives used have to be optimized to achieve a good performance from any specific application or design.

References

1 K. Zaghib, M. Armand and M. Gauthier, *J. Electrochem. Soc.*, 1998, **145**, 3135.
2 I. Exnar, L. Kavan, S. Y. Huang and M. Grätzel, *J. Power Sources*, 1997, **68**, 720.
3 A. Singhal, G. Skandan, G. Amatucci, F. Badway, N. Ye, A. Manthiram, H. Ye and J. J. Xu, *J. Power Sources*, 2004, **129**, 83.
4 B. O'Regan and M. Grätzel, *Nature*, 1991, **353**, 737.
5 A. Hagfeldt and M. Grätzel, *Acc. Chem. Res.*, 2000, **33**, 269.
6 Grätzel, *J. Photochem. Photobiol., A*, 2004, **164**, 3.
7 P. Bonhôte, A.-P. Dias, N. Papageorgious, K. Kalyanasundaraman and M. Grätzel, *Inorg. Chem.*, 1996, **35**, 1168.
8 T. Welton, *Chem. Rev.*, 1999, **99**, 2071.
9 C. Lagrost, D. Carrié, M. Vaultier and P. Hapiot, *J. Phys. Chem. A*, 2003, **107**, 745.
10 R. Hagiwara and Y. Ito, *J. Fluorine Chem.*, 2000, **105**, 221.
11 U. Schröder, R. G. Compton, F. Marken, S. D. Bull, S. G. Davies and S. Gilman, *J. Phys. Chem. B*, 2001, **105**, 1344.
12 D. R. McFarlane, J. Sun, J. Golding and P. Meakin, and M. Forsyth, *Electrochim. Acta*, 2000, **45**, 1271.
13 H. Randriamahazaka, C. Plesse, D. Teyssié and C. Chevrot, *Electrochem. Commun.*, 2003, **5**, 613.
14 H. Randriamahazaka, C. Plesse, D. Teyssié and C. Chevrot, *Electrochem. Commun.*, 2004, **6**, 299.
15 M. C. Buzzeo, R. G. Evans and R. G. Compton, *ChemPhysChem*, 2004, **5**, 1106.
16 P. Wang, S. M. Zakeeruddin, J.-E. Moser and M. Grätzel, *J. Phys. Chem. B*, 2003, **107**, 13280.
17 W. Kubo, S. Kambe, S. Nakade, T. Kitamura, K. Hanabusa and S. Yanagida, *J. Phys. Chem. B*, 2003, **107**, 4374.
18 P. Wang, S. M. Zakeeruddin, R. Humphry-Baker and M. Grätzel, *Chem. Mater.*, 2004, **16**, 2004.
19 F. Fabregat-Santiago, I. Mora-Seró, G. Garcia-Belmonte and J. Bisquert, *J. Phys. Chem. B*, 2003, **107**, 758.
20 A. Zaban, S. T. Aruna, S. Tirosh, B. A. Gregg and Y. Mastai, *J. Phys. Chem. B*, 2000, **104**, 4130.
21 H. Randriamahazaka, V. Noël and C. Chevrot, *J. Electroanal. Chem.*, 1999, **472**, 103.
22 F. Fabregat-Santiago, G. Garcia-Belmonte, J. Bisquert, P. Bogdanoff and A. Zaban, *J. Electrochem. Soc.*, 2002, **150**, E293.
23 B. E. Conway and W. G. Pell, *J. Electroanal. Chem.*, 2001, **500**, 121.
24 W. G. Pell and B. E. Conway, *J. Power Sources*, 2001, **96**, 57.
25 J. Bisquert, *J. Phys. Chem. B*, 2004, **108**, 2323.
26 J. Garcia-Cañadas, I. Mora-Seró, F. Fabregat-Santiago, J. Bisquert and G. Garcia-Belmonte, *J. Electroanal. Chem.*, 2004, **565**, 329.
27 J. Bisquert, G. Garcia-Belmonte and J. Garcia-Cañadas, *J. Chem. Phys.*, 2004, **120**, 6726.
28 J. van de Lagemaat, N.-G. Park and A. J. Frank, *J. Phys. Chem. B*, 2000, **104**, 2044.

29 Z. Zhang, S. M. Zakeeruddin, B. C. O'Regan, R. Humphry-Baker and M. Gra1tzel, *J. Phys. Chem. B*, 2005, **109**, 21818.
30 J. Bisquert, *Phys. Chem. Chem. Phys*., 2003, **5**, 5360.
31 M. Büttiker, *J. Phys.: Condens. Matter*, 1993, **5**, 9361.
32 J. Jamnik and J. Maier, *Phys. Chem. Chem. Phys*., 2001, **3**, 1668.
33 A. Hagfeldt, U. Björkstén and M. Grätzel, *J. Phys. Chem*., 1996, **100**, 8045.
34 G. Boschloo and D. Fitzmaurice, *J. Phys. Chem. B*, 1999, **103**, 7860.
35 F. Fabregat-Santiago, G. Garcia-Belmonte, J. Bisquert, G. Boschloo and A. Hagfeldt, *Sol. Energy Mater. Sol. Cells*, 2005, **87**, 117.
36 S. Kambe, S. Nakade, T. Kitamura, Y. Wada and S. Yanagida, *J. Phys. Chem. B*, 2002, **106**, 2967.
37 L. Kavan and M. Grätzel, *Electrochim. Acta*, 1995, **40**, 643.
38 G. Boschloo and D. Fitzmaurice, *J. Phys. Chem. B*, 1999, **103**, 2228.
39 F. Fabregat-Santiago, G. Garcia-Belmonte, J. Bisquert, A. Zaban and P. Salvador, *J. Phys. Chem. B*, 2002, **106**, 334.